Water Practice & Technology

IWA PUBLISHING

Water Practice & Technology Vol 18 No 11, 2884 doi: 10.2166/wpt.2023.174

Delineation of groundwater potential zones using electrical resistivity technique in Obudu basement terrain of Cross River State, Southeastern Nigeria

Ebong Dickson Ebong [a,*], Chimezie Ndunagum Emeka[b], Oualid Melouah[c], Rose Illa Ullah[a], Anthony Edet Ita[a] and Jamal Asfahani[d]

[a] Applied Geophysics Programme, Physics Department, University of Calabar, PMB 1115 Calabar, Cross River State, Nigeria
[b] Geology Department, University of Calabar, PMB 1115 Calabar, Cross River State, Nigeria
[c] Earth and Space Sciences Department, Faculty of Hydrocarbons, Renewable Energy and Earth and Space Sciences, University Kasdi Merbah Ouargla, Ouargla 30000, Algeria
[d] Geology Department, Atomic Energy Commission of Syria, P.O. Box 6091, Damascus, Syria
*Corresponding author. E-mail: dickebong@yahoo.co.uk; ebongdickson@unical.edu.ng

EDE, 0000-0002-5744-3887

ABSTRACT

Groundwater exploration in basement terrain can be somewhat challenging. Aquifer parameters like hydraulic conductivity and transmissivity can help in predicting groundwater potential zones in basement terrains. The vertical electrical sounding investigation that involved the Schlumberger configuration was employed to map the subsurface layers within the crystalline basement of the Obudu Complex, southeastern Nigeria. Secondary electrical resistivity data (Dar Zarrouk parameters) and a few pumping test-derived hydraulic parameters (i.e., transmissivity and hydraulic conductivity) were employed to develop empirical models. These models were used to predict hydraulic parameters at locations where only geoelectrical parameters (i.e., aquifer layer thickness and electrical resistivity) exist. Results showed that the northeastern part of the study area and areas located within zones of major faults displayed relatively higher values of hydraulic conductivity and transmissivity. The study area was classified into good, moderate, and poor groundwater potential aquifer zones. This integrated approach can be adopted in other areas with similar geology, where pumping test information is scarce or limited, as an alternative means of predicting aquifer properties and delineating groundwater potential zones for sustainable development and management of groundwater resources.

Key words: electrical anisotropy, electrical resistivity, hydraulic conductivity, Obudu-Nigeria, transmissivity

HIGHLIGHTS

- Electrical resistivity technique was used to estimate aquifer parameters in the Obudu basement.
- Empirical models derived were used to deduce these parameters elsewhere within the basement.
- Results show a good fit where both pumping test-derived and geoelectrical predicted values exist.
- It provided reliable site-specific and cost-effective alternatives to pumping test-derived parameters.

GRAPHICAL ABSTRACT

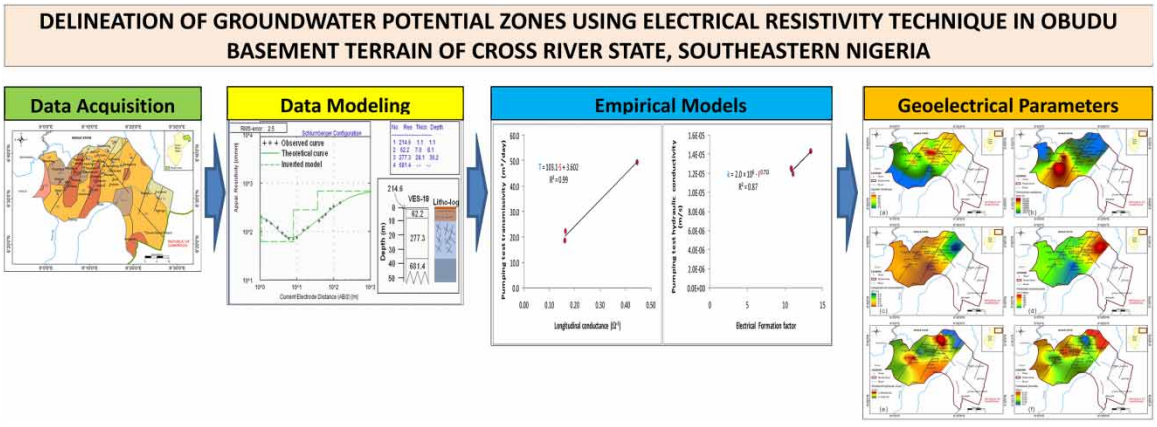

1. INTRODUCTION

The residents of the northeastern parts of Cross River State, Nigeria, domiciled within the basement terrain of the Obudu plateau, have over the years suffered from water scarcity problems. This critical situation is due to the nature of groundwater occurrence in basement terrain (Sarwade *et al.* 2007; Puranik 2009; Mondal 2021; Hassan *et al.* 2022), the low specific capacity of boreholes, consistent variations and discontinuities in aquifer properties (Limaye 2010), and other complexities such as irregular subsurface structural characteristics) associated with the exploration and quantitative assessment of the resources (Darko & Krásny 2003). Several boreholes within the area under investigation have failed due to limited knowledge and understanding of the structural, hydrogeological, hydrological, and geomorphological conditions of the basement environment by some borehole contractors (Mondal *et al.* 2008; Guevara-Mansilla *et al.* 2020; Ige *et al.* 2021). Groundwater transmission in fractured rocks depends mainly on the interconnectivity and extent of fractures, which are products of local and regional-scale tectonic activities, weathering, and lithology. Recent studies have shown that hard rock lithologies have specific individual hydrodynamic properties (Chandra *et al.* 2010; Courtois *et al.* 2010; Dewandel *et al.* 2011; Mondal *et al.* 2016; Ebong *et al.* 2021a; Lachassagne *et al.* 2021). For instance, the hydrodynamic properties of the saprolite layer have been reported to be capacitive, whereas the stratiform fissured layer displays transmissive properties (Lachassagne *et al.* 2021). In addition, unweathered granitic rocks possess low primary porosity and low hydraulic conductivity in contrast to metamorphic rocks that have lost their original hydrodynamic characteristics through metamorphic processes and have acquired secondary porosity that can facilitate groundwater transmission (Achtziger-Zupancik *et al.* 2017).

In this study, we propose to estimate aquifer parameters to facilitate groundwater exploration decisions and sustainable groundwater resources management within the northeastern part of Cross River State that constitutes the study area. These parameters include porosity, hydraulic conductivity, and transmissivity. Some of these parameters are derived conventionally from pumping tests, tracer test experiments, and grain size analysis from drilled boreholes. Although these methods are relatively expensive (i.e., the cost of borehole drilling and pumping tests), they have been used over the years and are relied upon to produce dependable results. Besides, the hydrogeologic conditions of interest for groundwater to occur in basement terrain, such as faults and fractures are to a certain extent localized (i.e., laterally limited) within the subsurface. Thus, aquifer properties derived from the pumping test of a particular borehole can result in inaccurate characterization when used to extrapolate or predict aquifer properties some few meters to a kilometer away from the borehole point (Sanderson & Zhang 1999). However, with few pumping test-derived hydraulic parameters and adequately constrained electrical resistivity sounding at these pumping test locations, empirical models can be developed and used to predict these parameters in the vicinity of the borehole and elsewhere within the study area where geoelectrical measurement information exists. The vertical electrical sounding (VES) technique when combined with hydrogeological measurements can provide a reliable alternative approach for the estimation of aquifer parameters. This approach has been utilized in resolving a variety of hydrological, hydrogeological, environmental and engineering problems (Obianwu *et al.* 2015; Guevara *et al.* 2017; Akpan *et al.* 2018; George *et al.* 2018; Arétouyap *et al.* 2019; Ndubueze *et al.* 2019; Asfahani & Ahmad 2020; Ebong *et al.* 2021b, 2023; Haq *et al.* 2022; Karthik *et al.* 2022), vadose zone infiltration rates, groundwater protective capacity and vulnerability assessments (Mhamdi *et al.* 2015; Akpan *et al.* 2016; Hussain *et al.* 2017), and geohydraulic parameter estimation (Ebong *et al.* 2014; Vogelgesang *et al.* 2020; Mahmud *et al.* 2022). More so, Asfahani & Al-Fares (2021) provided reliable estimates of hydraulic parameters within the Quaternary basaltic aquifer in the Deir Al-Adas area, southern Syria. The less-expensive geoelectrical resistivity method constitutes a rapid and versatile procedure that does not disturb the environment in any significant manner and can provide reliable results when adequately constrained (Akpan *et al.* 2015; Ebong *et al.* 2021a). This cost-effective technique is frequently used to resolve groundwater-related problems where good electrical resistivity contrasts exist between the saturated and unsaturated layers. Also, it is suitable for environmental and hydrogeological surveys in both sedimentary basins and hard rock terrains (Aleke *et al.* 2018; Mahmud *et al.* 2022). In spite of these advantages, geophysical data are fraught with errors, albeit the data acquisition may have been performed under favorable conditions. The errors are introduced into the results due to the unresolved ambiguity problem associated with converting geophysical data into representative geological models (Ebong 2012). The application of lithologic and other information derived from nearby boreholes as constraints during the VES forward modeling process remarkably minimize the ambiguity problems associated with one–dimensional (1D) modeling (Ebong *et al.* 2017; Bahammou *et al.* 2021).

This study aims to improve water security by effectively locating sustainable groundwater target zones and developing an empirical-based technique for estimating aquifer parameters in fractured rocks. The objective of the study is to generate aquifer empirical models based on modeled electrical resistivity data and few available pumping test information and apply the empirical models to estimate aquifer hydraulic properties (such as transmissivity, hydraulic conductivity, and fractional porosity) of fractured basement aquifer in other locations within the study area.

2. LOCATION AND GEOLOGY

2.1. Location

The study area falls within the Obudu Basement Complex (OBC) area in the northeastern part of Cross River State, Nigeria. It lies between Latitudes 6° 15′ 0″ and 6° 45′ 0′N and Longitudes 8° 56′ 0″ and 9° 30′ 0″ E; and occupies ~1,465 km^2 area (Ebong *et al.* 2021a) within southeastern Nigeria (Figure 1). It falls within the semi-temperate climatic region of West Africa, characterized by two dominant seasons, i.e., rainy and dry seasons. While the rainy season starts in April and gradually subsides in September, the dry season begins in October and terminates in March (Ebong *et al.* 2021a). During the dry season, the temperature within the area ranges from 26 to 32 °C and can drop to ~4 °C within the crest of plateau (~1,716 m above m.s.l); and ~10 °C in the adjourning area during the rainy season (Ebong *et al.* 2021a). Relative humidity varies from 40 to 80% (Edet & Okereke 2005). Annual rainfall ranges from 2,000 to 2,500 mm within adjourning areas and can rise to ~4,200 mm at the peak of the Plateau. The study area is composed of interlocking hill networks and elevation increases from about 200 m to approximately 1,800 m above m.s.l at the crest of the plateau (Figure 2).

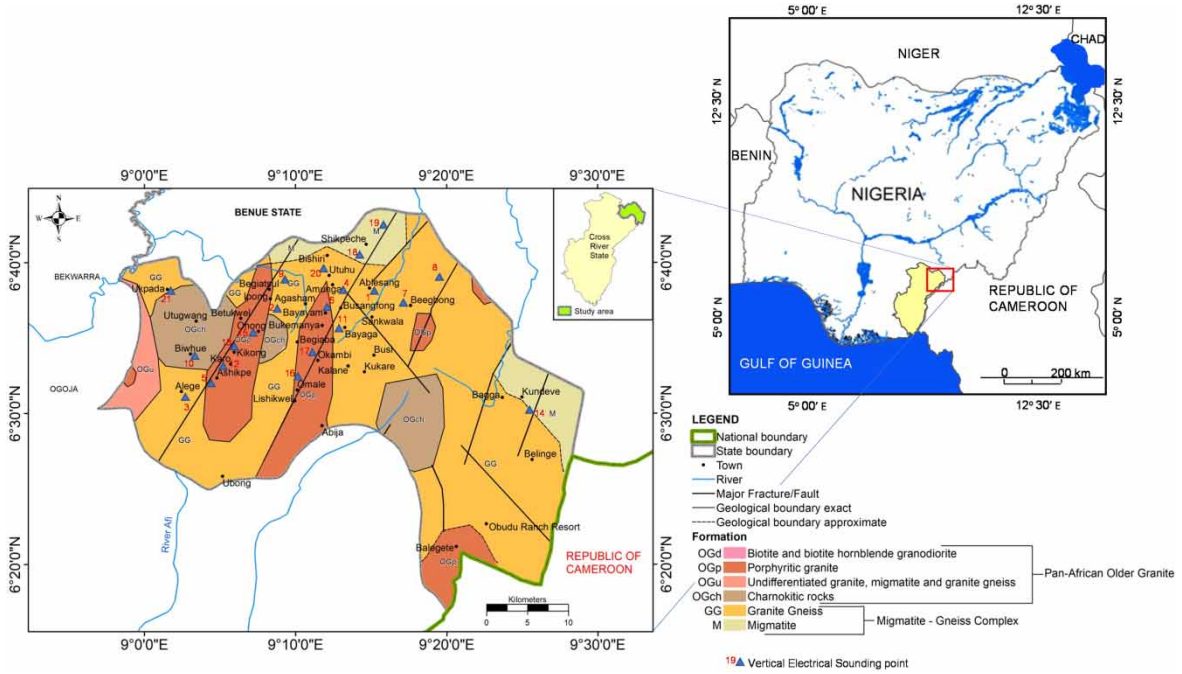

Figure 1 | Geologic map of study area showing VES points (adapted from Ebong *et al.* 2021a).

2.2. Geology and hydrogeology

The dominant rocks within the OBC are grouped into the Migmatitic Gneiss Complex and the Pan-African Older Granites (Ebong *et al.* 2021a). These rocks include migmatites, gneisses, undifferentiated granites, and schists. Details of the nature and characteristics of these rocks are well documented (Ekwueme 1990, 2003; Ukwang *et al.* 2003). The gneissic rocks have been intruded by pegmatite in several locations (Ekwueme 1994). At other locations, the gneisses have been folded and refolded with enclosed xenoliths while in some locations where schists are dominant, intense shearing, and fracturing due to thermal contacts have been reported

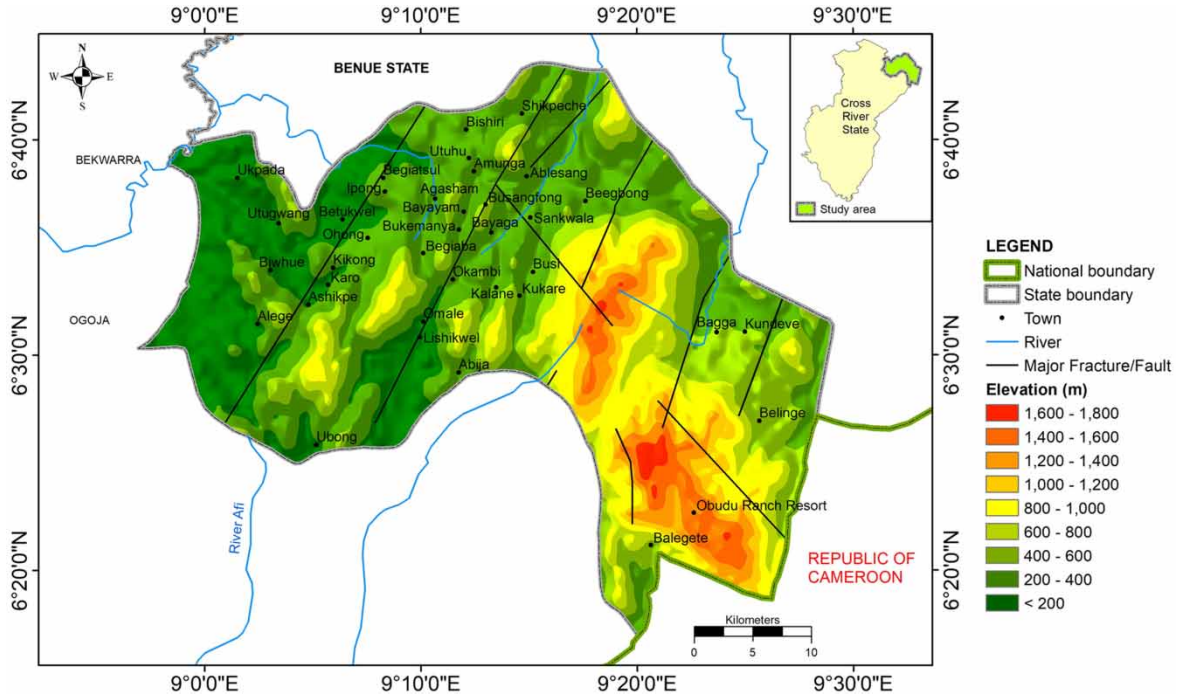

Figure 2 | Digital elevation model of the study area.

(Edem *et al.* 2016). Several weakly foliated boulders of garnet gneisses, charnockites, dolerite dykes on banded amphibolites having sharp contacts due to brittle deformation and massive quartz veins with multiple fractures have been reported (Oden *et al.* 2012; Ebong *et al.* 2021a).

Hydrogeologically, the study area depends on weathering and secondary tectonic activities for groundwater transmission and storage. Ebong *et al.* (2021a) identified potential aquifer types namely, the regolith aquifer type and the dolerite-intrusion-induced fracture-aquifer type within the OBC. Hence, the weathered and fractured zones constitute the main aquifer zones within the area and were mapped in this study. Since the aquifer zones are limited to the weathered and fractured column, which occur at relatively very shallow depths, the inhabitants of the area tend to depend on hand-dug wells and very few deep boreholes in the area which are often not functional, especially during the dry season. Edet & Okereke (2005) reported that the weathered overburden regolith (~38 m thick on average) and fractured basement rock aquifers can provide average permeability and transmissivity of $\sim 7.5 \times 10^{-1}$ m/day and 3.8×10^{-1} m^2/day, respectively. Groundwater-specific capacity and yield estimated from lineament density within the regolith wells were in the range of 40–270 m^3/day/m and 700–4,050 m^3/day, respectively (Edet & Okereke 2005). Static water levels in the area vary between 5 and 15 m and depths of hand-dug wells range from a few meters to ~15 m while tube wells may extend to ~50 m (Okereke *et al.* 1995).

3. METHODOLOGY

3.1. Materials and methods

The VES technique that involves measuring the difference in potential between the potential electrode pair arising from current injected into the ground through the current electrode pair was employed in this investigation (Bhattacharya & Patra 1968; Binley 2015; Ahmed *et al.* 2022; Chibuike *et al.* 2023). The Integrated Geo Instruments and Services (IGIS) signal enhancement resistivity meter (model SSR-MP-ATS) was utilized in measuring the earth resistance within the shallow subsurface. Twenty-one electric soundings were carried out using the Schlumberger array with current electrode separation (AB) that ranged from 2 to 500 m and sometimes up to 600 m in areas where accessibility is unlimited. Consequently, the potential electrode pair (MN) separation ranged between 0.5 and 20 m. The quality of the VES data was generally good, but in dry grounds where the contact resistance was high, water was used to moisten the ground around the electrodes, to reduce the contact resistance and enhance the current input in such areas (Uhlemann *et al.* 2018; Ebong *et al.* 2021a). Water

samples from boreholes and hand-dug wells closest to the VES points were collected and the electrical conductivity (EC) was measured using a hand-held conductivity meter.

3.2. Data analysis and interpretation

The apparent electrical resistivity (ρ_a) values were plotted against their corresponding half-current electrode spacing (AB/2) on a bi-log graph paper. The resulting VES curves were interpreted in terms of layer electrical resistivity and actual depths and/or thicknesses of rocks through computer-assisted forward modeling. The electrical resistivity and depth values of each geoelectric layer used as starting model during the forward modeling phase were constrained using lithologic data (i.e., layer electrical resistivities and thicknesses) from available boreholes closest to the VES points. The geologic constraints were meant to reduce the ambiguity problem associated with the non-uniqueness associated with VES data interpretation (LaBrecque *et al.* 1996). The observed apparent electrical resistivity values for each VES point were compared during the iteration process with the theoretically generated values until good fits were realized after a certain number of iterations with minimum root mean square errors of <2.5% (Inman 1975). The 1D geoelectric models were produced using the RESIST code (Vander Velpen 1988; Vander Velpen & Sporry 1993). Figure 3 shows samples of the 1D electrical resistivity models and their correlation with lithologic logs. The interpreted output provides geoelectric layer parameters (i.e., electrical resistivity and thickness) that were used in estimating hydrogeological parameters like transmissivity and hydraulic conductivity.

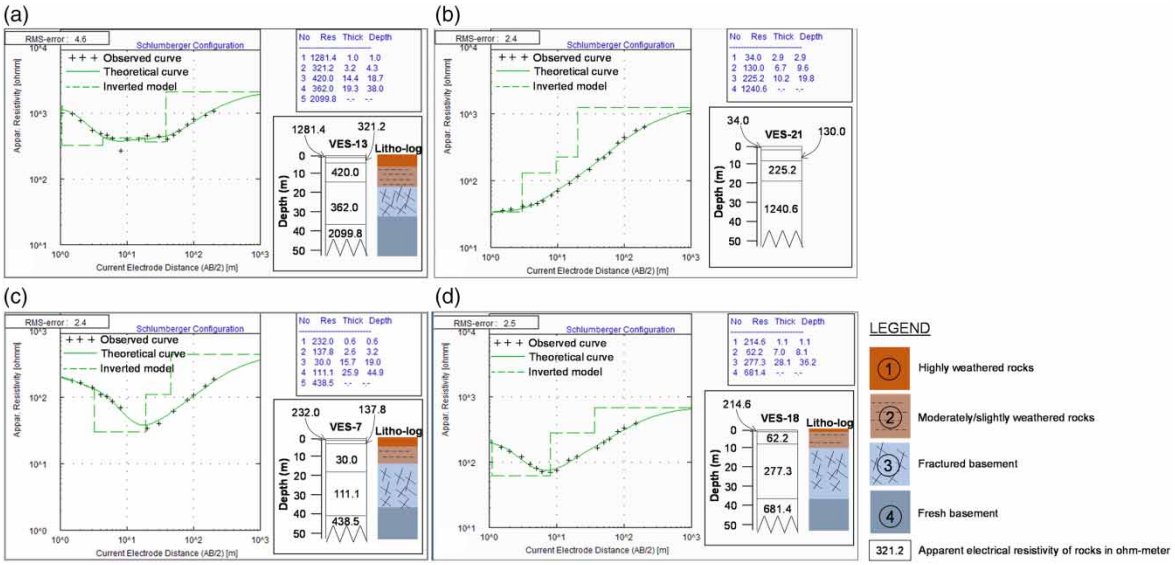

Figure 3 | Samples of VES curves and 1D electrical resistivity models correlated with some lithologic logs from drilled boreholes. (1) The highly weathered rocks (top layer) constitute predominantly reddish at top from 0.2 to 2.0 m composed of gravely-clays and grades into reddish-yellow sandy-clay (regolith) with lots of quartz grains. (2) The moderate/slightly weathered layer constitutes the laminated saprolite layer composed of brownish coarse sand clastic texture with preserved fissures from orthogneissic granites and about ~10 m thick. (3) The fractured basement constitutes fissured granite gneisses with numerous fragments of porphyritic granite clastics. (4) The fresh basement constitutes unweathered granite gneisses, migmatites, and porphyritic granites. The apparent electrical resistivities were interpreted based on information from Telford *et al.* (1990); Reynolds (2011) and Ebong *et al.* (2021a).

Different combinations of layer electrical resistivity (ρ) and thickness (h) have been applied in hydrogeological investigations. Maillet (1947) referred to these combinations as Dar Zarrouk (D-Z) parameters. These D-Z parameters consist of the longitudinal conductance (S) that relates to electric conductance parallel to the face of a unit cross-sectional area and the transverse resistance (TR) which corresponds to the resistance normal to the face for a unit cross-sectional area (Maillet 1947; Batte *et al.* 2010; Mahmud *et al.* 2022). According to Gowd (2004), S can be used to adequately assess the properties of a thin conducting layer and is quantitatively expressed as

$$S = \sum_{i=1}^{N} \frac{h_i}{\rho_i} \tag{1}$$

where h and ρ are the layer electrical resistivity and thickness, and $i = 1, 2, 3 \ldots N$th layer. Such thin and highly conductive structures in hard rock environments are usually fractures/faulted rock columns and can store and transmit water. Such locations within the hard rock terrain have been reported to have high groundwater potential (Naidu *et al.* 2021). TR, the product of h and ρ (Niwas & Singhal 1981; Okonkwo & Ugwu 2015) is represented by

$$\mathrm{TR} = \sum_{i=1}^{N} h_i * \rho_i \tag{2}$$

where h and ρ are the layer electrical resistivity and thickness, and $i = 1, 2, 3 \ldots N$th layer. The average longitudinal resistivity (ρ_L) (Equation (3)) and average transverse resistivity (ρ_T) (Equation (4)) are other geoelectrical parameters that can be derived from the *D-Z* parameters (Maillet 1947) and are defined as;

$$\rho_\mathrm{L} = \frac{\sum h_i}{S} \tag{3}$$

$$\rho_\mathrm{T} = \frac{\mathrm{TR}}{\sum h_i} \tag{4}$$

The variation expressed by these parameters is a measure of the anisotropic nature of the environment. Considering the resistivity across the bedding plane, i.e., transverse resistivity (ρ_T) and that parallel to the bedding (Maillet 1947; Mazáč *et al.* 1985), i.e., the longitudinal resistivity (ρ_L), the dimensionless electrical anisotropy (λ) is given as

$$\lambda = \sqrt{\frac{\rho_\mathrm{T}}{\rho_\mathrm{L}}} \tag{5}$$

In anisotropic geological units, λ is >1 since electrical resistivity is greatest in the transverse direction (Yeboah-Forson & Whitman 2014). These parameters are used to characterize groundwater potential in hard rock environments where groundwater availability depends on weathered and fractured conduits.

The formation factor (F) is a fundamental parameter when considering the electrical properties of rocks. It provides a measure of the influence that the pore structure offers on the flow and/or resistance of fluid. Studies have shown that changes in F are occasioned by temperature, lithological characteristics, porosity (ϕ), extent of saturation and pore fluid resistivity and can affect the electrical resistivity response of the formation (Ziarani & Aguilera 2012; Ebong *et al.* 2014). Archie (1942) empirical relationship of F for a saturated rock is given by

$$F = a.\phi^{-m} \tag{6}$$

where a represents the tortuosity factor and m is the cementation exponent. However, in fractured rock aquifers, the relationship between a, m, and ϕ that describes the nature of the saturated formation is a complicated phenomenon, since rocks are not homogeneously fractured equally in all directions. Consequently, it becomes difficult to effectively predict or determine these parameters from well-cuttings. Core analysis that can serve as an alternative approach is expensive to perform. However, Equation (7) relates F, the electrical resistivity of bulk saturated geologic formation (ρ_b), and electrical resistivity of pore water (ρ_w).

$$F = \frac{\rho_\mathrm{b}}{\rho_\mathrm{w}} \tag{7}$$

This relation provides a rather simplistic but relevant way of determining F since the EC of borehole water can be measured using a hand-held conductivity meter in micro-mho per centimeter (μmho/cm). The inverse of conductivity is resistivity; hence, the measured borehole water EC can be converted to electrical resistivity in ohm-meter (Ωm), using Equation (8). Since ρ_b can be derived from geoelectrical resistivity measurements and ρ_w from the water wells, F of saturated rock formation can be estimated using the following equation.

$$\rho_\mathrm{w}(\Omega\mathrm{m}) = \frac{10,000}{\mathrm{EC}(\mu\mathrm{mho/cm})} \tag{8}$$

One of the significance of the formation factor is that it can be employed in the estimation of hydraulic conductivity of the saturated medium (Kelly 1977). Hydraulic conductivity is the capacity of an aquifer to transmit water through fractures and pore spaces under the influence of hydraulic gradient (Lobo-Ferreira *et al.* 2005). It determines the ability of a geologic formation to transmit a unit volume of groundwater in unit time at the existing viscosity through a unit cross-sectional area, measured perpendicularly to the flow direction, under a hydraulic gradient of unit change in the head through a unit flow length (Lohman 1979; Maliva & Missimer 2012). In other words, it is a coefficient of permeability that measures the ease with which water flows through a medium and depends on the properties of the medium, such as pore fluid density and viscosity, and acceleration of gravity (Vukovic & Soro 1992). In fractured basement aquifers, hydraulic conductivity may vary from 0 to 1,000 m/day (Kruseman & de Ridder 1990; Gnanachandrasamy *et al.* 2019; Saravanan *et al.* 2019) and depends on the intrinsic permeability, fracture width, density and interconnectivity of fractures, and hydraulic gradient. The Kozeny–Carman method is widely used to derive hydraulic conductivity but falls short in heterogeneous strata (Zhu *et al.* 2016).

In order to adequately characterize the Obudu fractured basement aquifer, we considered the relationships between pumping test transmissivity and the measured and computed secondary aquifer parameters, i.e., ρ_b, ρ_w, TR, and S (Figure 4). The correlation revealed a strong positive correlation between T vs S (0.9937) and ρ_b vs TR (0.9849), a strong negative correlation between T vs TR (−0.9606), TR vs S (−0.9234), T vs ρ_b (−0.8978), and S and ρ_b (−0.8429). A medium positive correlation was observed between ρ_b vs ρ_w (0.6358) while poor positive correlation was observed between TR and ρ_w (0.4924). Also, a poor negative correlation was observed between T vs ρ_w (−0.2309) and ρ_w vs S (−0.1205). Hence, the parameters with the strongest positive were used to establish the empirical relationship, i.e., T and S derived from VES (Equation (9)). The second empirical related k and F derived from ρ_b and ρ_w (Equation (10)).

$$T = 103.1 \cdot S + 3.602, \ (R^2 = 0.99) \text{ (Figure 5(a))} \tag{9}$$

$$k = 2.0 \times 10^{-6} \cdot F^{0.753}, \ (R^2 = 0.87) \text{ (Figure 5(b))} \tag{10}$$

	T	S	TR	ρb	ρw
T	1				
S	0.993709	1			
TR	-0.96055	-0.92336	1		
ρb	-0.89784	-0.84288	0.984879	1	
ρw	-0.23093	-0.12051	0.492412	0.635753	1

Figure 4 | Pearson correlation matrix showing the relationship between the aquifer parameters.

where T is the pumping test-derived transmissivity, i.e., the product of hydraulic conductivity and aquifer thickness (Younger 2007) expressed in m^2/day, and k is pumping test-derived hydraulic conductivity expressed in m/s. Equations (9) and (10) were used to determine transmissivity and hydraulic conductivity for all VES locations where there are no boreholes or the aquifer hydraulic parameters are unknown. However, the apparent limitation of the empirical equations lies in the few pumping test information available within the area. In areas where more pumping test-derived information (i.e., transmissivity and hydraulic conductivity) are available, they can be included in generating the models to provide better estimates of these parameters.

$$T = kh \tag{11}$$

Based on the strong statistical significance of these models (i.e., the strong relationship between the variables), they can be applied at any location within the Obudu area and environs where geoelectrical data exist, to directly evaluate the transmissivity and hydraulic conductivity of the aquifer to enhance the selection of appropriate sites that can provide optimum groundwater yield to boreholes. The application of the models can be summarized in the following steps;

Step 1: Acquire geoelectrical data for the proposed survey area

Step 2: Compute the longitudinal conductance (S) of the formation
Step 3: Determine the transmissivity of the aquifer formation by substituting the computed longitudinal conductance value into Equation (9).
Step 4: Determine the hydraulic conductivity of the aquifer formation using Equation (11) from known saturated aquifer thickness.

However, if the formation factor is estimated based on Equations (7) and (8), then Equations (10) and (11) can be used to evaluate the hydraulic conductivity and transmissivity, respectively.

The fractured basement aquifer fractional porosity (ϕ) was determined by combining Equations (6) and (7)

$$\phi = \left(\frac{a\rho_w}{\rho_b}\right)^{\frac{1}{m}} \tag{12}$$

where a and m are equivalent to 1.4 and 1.58, respectively, for rocks with <4% porosity including igneous and metamorphosed sediments (Keller 1987). Porosity is a measure of the capacity by which a saturated thickness can store and transmit water. This procedure that involves estimating transmissivity from apparent formation factor eliminates the effect of aquifer water resistivity changes while utilizing the information provided by these changes in its estimation (K'Orowe *et al.* 2011; Ebong *et al.* 2014).

4. RESULTS

The electrical resistivity models provided the geoelectric layer parameters ρ and h values that were used in evaluating the *D-Z* parameters (Table 1). The *D-Z* parameters i.e., TR and longitudinal conductance range from 3,266.64 to 64,338.35 Ωm^2 and 0.04 to 0.85 Ω^{-1}, respectively. Figure 6(a) and 6(b), reveal the spatial distribution of both TR and longitudinal conductance values. The ρ_L values ranged from 54.33 to 587.73 Ωm while ρ_T varied

Table 1 | Results of 1D electrical resistivity models

	Coordinates in degrees		Resistivity (Ωm)					Thickness (m)			
VES points	Longitude	Latitude	ρ_1	ρ_2	ρ_3	ρ_4	ρ_5	h_1	h_2	h_3	h_4
1	9.248	6.638	715.6	44.4	150.5	1,508.7	–	0.7	12.8	27.5	–
2	9.178	6.621	147.3	38.6	214.1	9,427.5	–	1.3	4.8	49.5	–
3	9.041	6.524	149.2	28.2	437.7	1,039.7	1,426.7	1.1	5.1	10.3	25.6
4	9.208	6.642	181.2	567.8	143.0	2,401.5	–	0.3	4.6	35.4	–
5	9.080	6.539	430.6	3,020	270.0	943.1	1,684.3	0.9	4.1	17.3	36.3
6	9.200	6.611	215.3	58	208.1	1,146.2	–	1.8	12.6	45.9	–
7	9.294	6.619	232	137.8	30.0	137.1	438.5	0.6	2.6	15.7	25.9
8	9.311	6.634	157.1	14.1	100.0	1,535.0	–	3.3	6.6	36.5	–
9	9.138	6.637	105.3	805.9	252.0	2,278.6	–	0.2	12.5	36.3	–
10	9.051	6.566	1,381	353.3	142.8	1,468.8	–	2.4	9.0	19.7	–
11	9.196	6.597	327.4	37.3	272.7	1,802.7	–	2.2	4.3	35.1	–
12	9.095	6.554	1,073.5	273.1	154.7	1,127.3	4,546.2	1.3	4.3	34.2	50.1
13	9.099	6.568	1,281.4	321.2	420.0	362.0	2,099.8	1.0	4.3	18.7	38
14	9.417	6.518	336.9	889.7	495.3	3,329.3	–	0.2	13.8	24.3	–
15	9.126	6.591	1,493.1	144.7	1,624.2	1,348.8	–	5.9	11.0	27.3	–
16	9.191	6.558	744.5	228.3	1,139.0	878.3	–	1.2	35.9	6.0	–
17	9.184	6.545	685.5	236.39	1,558.1	1,911.4	–	2.2	7.5	14.0	–
18	9.245	6.687	214.6	62.2	277.3	681.4	–	1.1	7.0	28.1	–
19	9.251	6.699	161.2	51.3	155.4	3,632.6	–	1.4	6.5	35.5	–
20	9.193	6.649	884.6	483.3	156.4	2,295.3	–	1.9	8.4	16.0	–
21	9.025	6.637	34.0	130.0	225.2	1,240.6	–	2.9	6.7	10.2	–

between 91.84 and 1,238.50 Ωm (Table 2). The electrical anisotropy that describes the variation of electrical resistivity of subsurface rocks and formations laterally and vertically (Youssef 2020) ranged between 1.0 and 2.0 and was observed to have been influenced by geologic and topographic conditions. It describes the directional dependence of EC or its inverse electrical resistivity of subsurface rocks and formations. The farther away the value of the coefficient of the electrical anisotropy of a medium is from unity, the greater the heterogeneity of the medium. Table 3 presents the results of aquifer parameters estimated from hydrogeologic measurements and 1D electrical resistivity models, and the summary of the statistics. Empirical relationships between the pumping test-derived parameters available in three locations where VES were performed, were used to develop the two site-specific models. These models were used to predict transmissivity and hydraulic conductivity at other unknown locations where VES data were acquired. The standard deviation statistic indicator was used to measure the reliability of the hydrogeologic parameters. It shows that the estimated parameters are clustered closely around their respective mean values (i.e., low standard deviations), hence, indicating more reliability of the estimates (Table 3). The empirical models show a good correlation with R^2 of 0.99 and 0.87 for the transmissivity and hydraulic conductivity models, respectively (Figure 5(a) and 5(b)). The aquifer electrical resistivity value was compared graphically with aquifer water resistivity measured from existing boreholes adjacent to the VES locations to establish an empirical model for hard rock aquifers (Figure 5(c)). The correlation coefficient revealed a strong relationship between both parameters. From the plot, the slope represents the average value of *F*. The predicted transmissivity also shows a good correlation with the TR computed for the area with a correlation coefficient of 0.76 (Figure 5(d)). The spatial distributions of aquifer thickness, TR, longitudinal conductance, predicted transmissivity and hydraulic conductivity, and fractured rock fractional porosity were represented in Figure 6. The fractured basement aquifer thickness map shows the spatial distribution across the area with minimum aquifer thickness at VES-17 while maximum aquifer thickness was observed at VES-2. The hydraulic conductivity within the hard

Table 2 | Estimated Dar–Zarrouk parameters and electric anisotropy

	Coordinates in degrees						
VES points	Longitude	Latitude	TR (Ωm^2)	S (Ω^{-1})	ρ_L (Ωm)	ρ_T (Ωm)	λ
1	9.248	6.638	5,207.99	0.47	86.87	127.02	1.2
2	9.178	6.621	10,974.72	0.36	152.59	197.39	1.1
3	9.041	6.524	31,432.57	0.24	178.10	746.62	2.0
4	9.208	6.642	7,728.44	0.26	156.62	191.77	1.1
5	9.080	6.539	51,675.07	0.11	552.77	881.83	1.3
6	9.200	6.611	10,670.13	0.45	135.15	176.95	1.1
7	9.294	6.619	4,519.37	0.73	61.06	100.88	1.3
8	9.311	6.634	4,261.49	0.85	54.33	91.84	1.3
9	9.138	6.637	19,242.41	0.16	303.49	392.70	1.1
10	9.051	6.566	9,307.26	0.17	188.29	299.27	1.3
11	9.196	6.597	10,452.44	0.25	165.93	251.26	1.2
12	9.095	6.554	64,338.35	0.28	318.26	715.67	1.5
13	9.099	6.568	24,272.56	0.16	378.83	391.49	1.0
14	9.417	6.518	24,381.03	0.07	587.73	636.58	1.0
15	9.126	6.591	54,741.65	0.10	456.71	1,238.50	1.6
16	9.191	6.558	15,923.37	0.16	262.60	369.45	1.2
17	9.184	6.545	25,094.43	0.04	539.59	1,058.84	1.4
18	9.245	6.687	8,463.59	0.22	165.30	233.80	1.2
19	9.251	6.699	6,075.83	0.36	119.29	140.00	1.1
20	9.193	6.649	8,242.86	0.12	215.87	313.42	1.2
21	9.025	6.637	3,266.64	0.18	108.72	164.98	1.2
Minimum			3,266.64	0.04	54.33	91.84	1.0
Maximum			64,338.35	0.85	587.73	1,238.50	2.0

Table 3 | Estimated aquifer parameters from geoelectrical and pumping test data and their basic statistics

Location	VES points	Coordinates in degrees							Pumping test		Predicted	
		Longitude	Latitude	ρ_b (Ωm)	ρ_w (Ωm)	h_a (m)	F	ϕ	T (m^2/day)	k (m/s)	T_p (m^2/day)	k_p (m/s)
Ablesang	1	9.248	6.638	150.5	9.8	28	15.4	0.22	–	–	52.3	1.56×10^{-5}
Agasham	2	9.178	6.621	214.1	18.5	50	11.6	0.26	–	–	41.2	1.26×10^{-5}
Alege	3	9.041	6.524	437.7	40.0	10	10.9	0.27	–	–	28.0	1.21×10^{-5}
Amunga	4	9.208	6.642	143.0	11.4	35	12.6	0.25	–	–	30.1	1.35×10^{-5}
Ashikpe	5	9.080	6.539	270.0	18.5	17	14.6	0.23	–	–	14.5	1.50×10^{-5}
Bayayam	6	9.200	6.611	208.1	19.2	46	10.8	0.28	49.6	1.25×10^{-5}	49.6	1.20×10^{-5}
Beegbong	7	9.294	6.619	137.1	11.4	26	12.1	0.26	–	–	79.2	1.30×10^{-5}
	8	9.311	6.634	100.0	9.9	37	10.1	0.29	–	–	91.7	1.14×10^{-5}
Begiatsul	9	9.138	6.637	252.0	22.7	36	11.1	0.27	18.5	1.19×10^{-5}	20.2	1.22×10^{-5}
Biuhwe	10	9.051	6.566	142.8	10.2	20	14.0	0.23	–	–	20.6	1.46×10^{-5}
Bukemanya	11	9.196	6.597	272.7	25.6	35	10.6	0.28	–	–	29.5	1.19×10^{-5}
Karo	12	9.095	6.554	154.7	11.2	34	13.8	0.24	–	–	32.7	1.44×10^{-5}
Kikong	13	9.099	6.568	362.0	23.3	38	15.6	0.22	–	–	20.5	1.58×10^{-5}
Kundeve	14	9.417	6.518	495.3	31.3	24	15.8	0.22	–	–	10.3	1.60×10^{-5}
Ohong	15	9.126	6.591	144.7	14.1	11	10.3	0.28	–	–	13.6	1.16×10^{-5}
Okambi	16	9.191	6.558	228.3	16.9	36	13.5	0.24	22.3	1.43×10^{-5}	20.5	1.42×10^{-5}
	17	9.184	6.545	236.39	16.9	8	13.9	0.23	–	–	8.1	1.45×10^{-5}
Shikpeche	18	9.245	6.687	277.3	15.4	28	18.0	0.20	–	–	26.2	1.76×10^{-5}
	19	9.251	6.699	155.4	15.4	36	10.1	0.29	–	–	41.1	1.14×10^{-5}
Udigie	20	9.193	6.649	156.4	12.2	16	12.8	0.25	–	–	16.2	1.37×10^{-5}
Ukpada	21	9.025	6.637	225.2	20.0	10	11.3	0.27	–	–	22.4	1.24×10^{-5}
Minimum				100.0	9.8	8	10.1	0.20	18.5	1.19×10^{-5}	8.1	1.14×10^{-5}
Maximum				495.3	40.0	50	18.0	0.29	49.6	1.43×10^{-5}	91.7	1.76×10^{-5}
Average				226.8	17.8	28	12.8	0.25	30.1	1.29×10^{-5}	31.8	1.36×10^{-5}
Standard Deviation				102.1	7.6	12	2.2	0.03	17.0	1.27×10^{-6}	21.6	1.76×10^{-6}

rock area is ranged between 1.14×10^{-5} and 1.76×10^{-5} m/s (Table 3). The observed results were within the range of 10^{-6}–10^{-5} m/s for fractured metamorphic rocks (Freeze & Cherry 1979; Shapiro *et al.* 2015). The range of values for fractional porosity and predicted transmissivity as shown in Table 3 are 0.20–0.29 and 8.1–91.7 m^2/day, respectively. The observed values of ϕ are adequate for fractured basement aquifers (Table 3). However, this range of porosity value is higher than the 0.00–0.10 range reported by Freeze & Cherry (1979) for fractured rocks. These high values are expected, since the estimation was based on the saturated thickness. However, based on conventional porosity classification of Etu-Efeotor (1997), ϕ is within the very good (i.e., 0.10–0.30) range (Table 4).

Table 5 presents the results of correlation analysis performed on transmissivity and hydraulic conductivity data from pumping test experiments at three specific borehole locations, juxtaposed with the corresponding values predicted via the hydro-geoelectrical technique at the same spatial coordinates, yielded correlation coefficients (R^2) of 0.98 and 0.89, respectively. Furthermore, an error analysis was performed on the hydraulic parameters, specifically transmissivity and hydraulic conductivity. The root mean square error (RMSE) and mean absolute percentage error (MAPE) were calculated to evaluate the accuracy of the predictions. For transmissivity, the RMSE and MAPE were determined to be 1.439 and 5.807, respectively. In the case of hydraulic conductivity, the corresponding values were 3.59×10^{-7} and 0.027, respectively. These low error values demonstrate the high precision of the predictive models used in estimating these hydraulic parameters. The accuracy of the predictions was assessed by calculating the percentage accuracy, which was observed to be 94.19 and 99.97%, respectively, for transmissivity and hydraulic conductivity. These results highlight the robustness and reliability

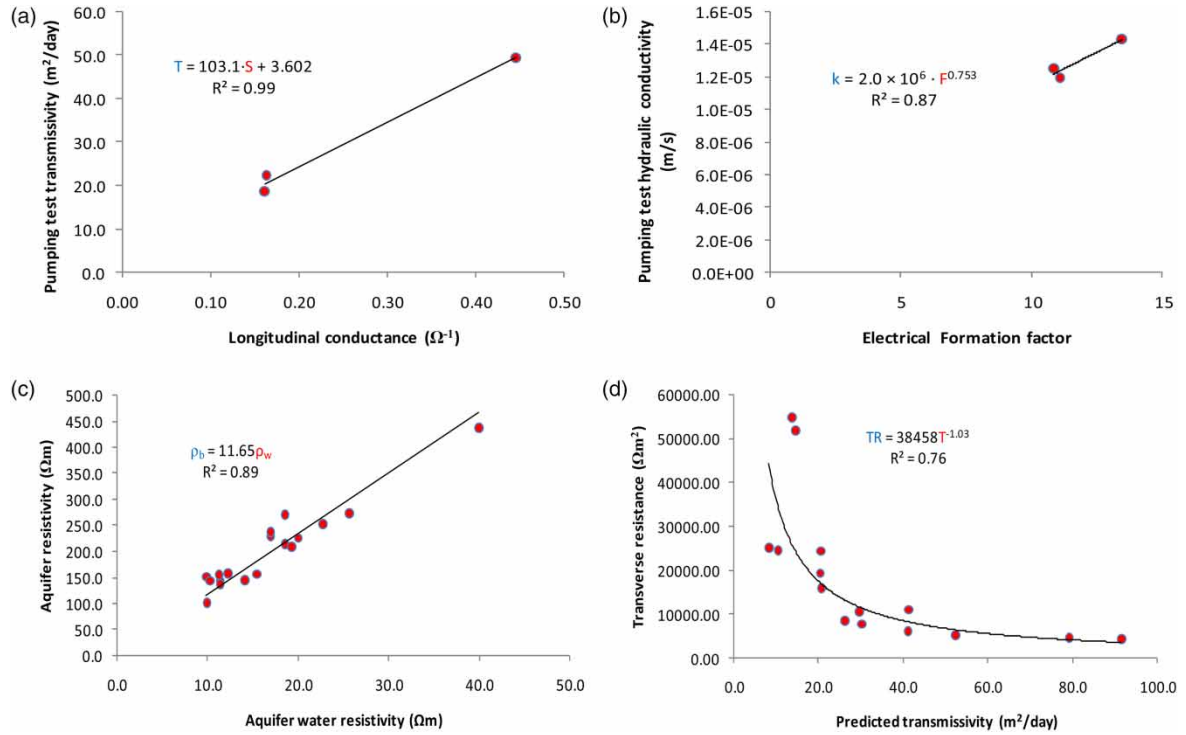

Figure 5 | Empirical relationships between (a) pumping test-derived transmissivity and longitudinal conductance, (b) pumping test-derived hydraulic conductivity and electrical resistivity formation factor, (c) aquifer resistivity and aquifer water resistivity, and (d) transverse resistance and predicted transmissivity.

of the employed predictive models in accurately characterizing the hydraulic parameters within the area under investigation.

5. DISCUSSION

5.1. Aquifer characterization of the OBC

Due to the cost-effectiveness and speed of the electrical resistivity technique, it permits greater spatial coverage and provides valuable pilot information that is needed for rapid aquifer characterization decisions. Aquifer characterization provides information on aquifer parameters and numerical models required for groundwater resources management, sustainability and prediction. These parameters that including the *D-Z* parameters, hydraulic conductivity, porosity, and transmissivity were evaluated within the OBC. TR values were observed to increase from the northern segment toward the south (Figure 6(b)). The low TR values within the northern portion correlated geologically with the portion of the study area dominated by migmatitic rocks. The migmatites have been subjected to intense weathering processes leading to reduced resistivity values of the formations within this area. TR values tend to show high values toward the south, around the massive porphyritic granite dominant terrain. On the other hand, *S* values were observed to increase from the western segment toward the northeastern part of the study area where it attained its maximum value (Figure 6(c)). The high *S* values are dominant within the parts where gneissic rocks have been intensely fractured and the aquifer formation electrical resistivity values within these areas have been reduced due to groundwater transmission. Crystalline basement terrains are usually dominated by episodes of faulting, fracturing, and intrusions leading to weathering of preexisting rocks. These processes alter the configuration and characteristics of crystalline rocks leading to heterogeneity in their electrical resistivity signatures. This phenomenon is responsible for the variations in electrical anisotropy within the area.

Figure 5(c) provides an empirical model of the aquifer formation due to ρ_b and ρ_w in the area, presented as

$$\rho_b = 11.65\rho_w \tag{13}$$

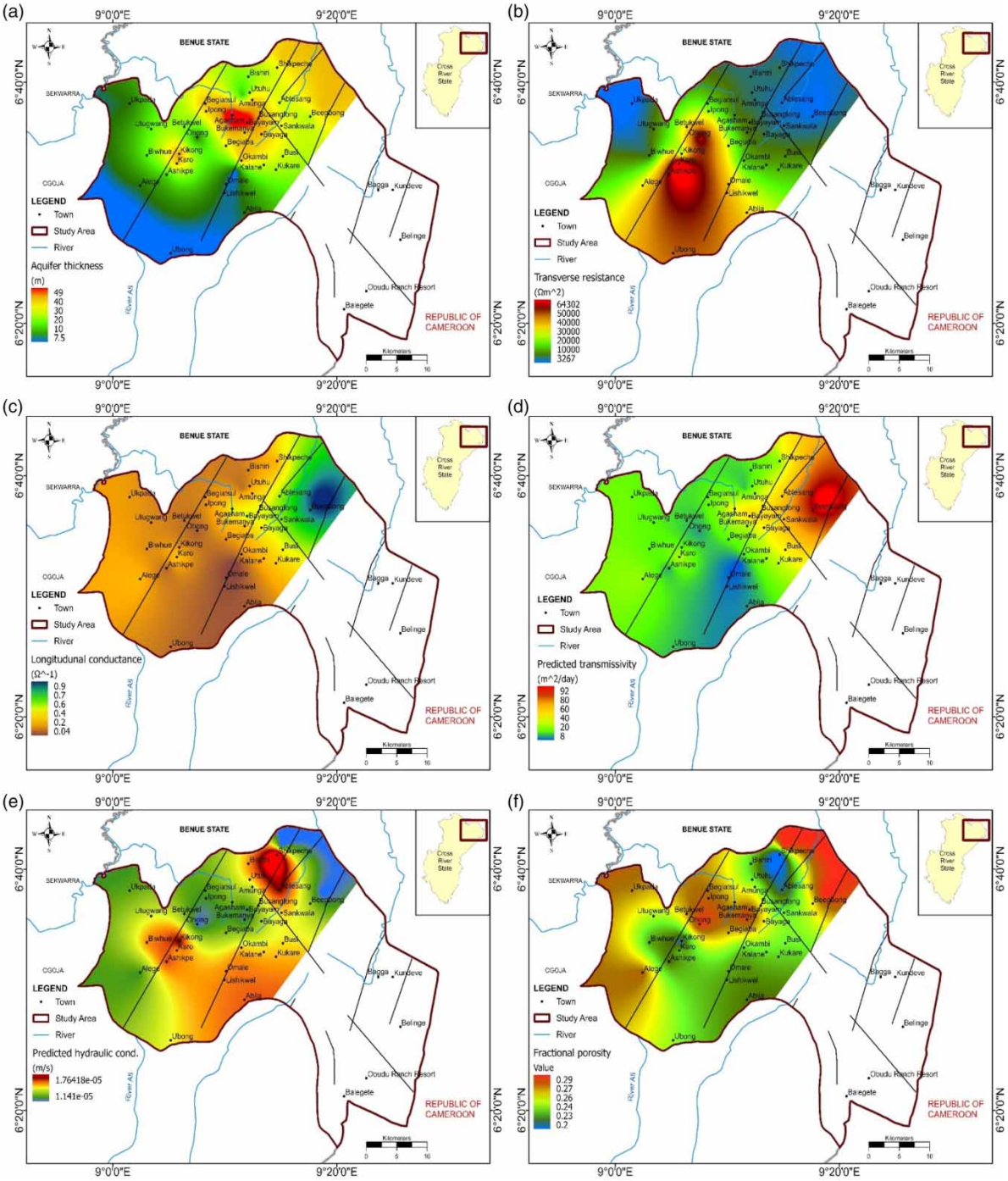

Figure 6 | Maps showing the spatial distribution of some aquifer parameters; (a) aquifer thickness, (b) transverse resistance, (c) longitudinal conductance, (d) predicted transmissivity (e) predicted hydraulic conductivity and (f) fractured basement aquifer fractional porosity.

Equation (13) gives the average F value as 11.65 – the slope of the equation. The lowest value of F was observed around VES-8 and VES-19 while relatively high values were observed at area (VES-18). The northern segment and areas located along major fault zones were notable portions with relatively high hydraulic conductivity (Figure 6(e)). The networks of fractures that provide semi-confined aquifers within the area are interconnected adequately which allows groundwater circulation (Ebong *et al.* 2014, 2021a; Ekwok *et al.* 2020). Lower values of k were observed around some locations within the central part sandwiched between the two dominant parallel faults and the western segments of the study area. The lower values that are dominant, especially within the

Table 4 | Groundwater potential classification

S/N	Locations	Parameters			Groundwater potential
		Range of resistivity (Ωm)	Aquifer thickness range (m)	Transmissivity (m^2/day)	
1	VES-1, VES-2, VES-6, VES-7, VES-8 and VES-19	100–214	26–50	>40	Good
2	VES-3, VES-4, VES-5, VES-9, VES-10, VES-11, VES-12, VES-13, VES-16, VES-18, VES-20 and VES-21	143–438	10–38	<40–15	Marginal
3	VES-14, VES-15 and VES-17	145–495	8–24	<15	Poor

Table 5 | Available aquifer parameters, their corresponding predicted values and statistical analysis

S/N	Parameter	VES-6	VES-9	VES-16	R^2	RMSE	MAPE	Accuracy (%)
1	Aquifer electrical resistivity, ρ_b (Ωm)	208	252	228.3	–	–	–	–
2	Saturated aquifer thickness, h_a (m)	46	36	36	–	–	–	–
3	Longitudinal conductance, S (Ω^{-1})	0.45	0.16	0.16	–	–	–	–
4	Transverse resistance, TR (Ωm^2)	10,670.1	19,242.4	15,923.37	–	–	–	–
5	Electrical formation factor	10.8	11.1	13.5	–	–	–	–
6	Aquifer transmissivity derived from pumping test, T (m^2/day)	49.6	18.5	22.3	0.99	1.43895	5.807	94.19
7	Predicted aquifer transmissivity from geoelectric sounding, T_p (m^2/day)	49.6	20.2	20.5				
8	Aquifer hydraulic conductivity derived from pumping test, k (m/s)	1.25×10^{-5}	1.19×10^{-5}	1.43×10^{-5}	0.89	3.5×10^{-7}	0.027	99.97
9	Predicted aquifer hydraulic conductivity from geoelectric sounding, k_p (m^2/day)	1.20×10^{-5}	1.22×10^{-5}	1.42×10^{-5}				

R^2, correlation coefficient; RMSE, root mean square error; MAPE, mean absolute percentage error.

western part of the landscape are due to minor occurrence of fracture networks. Also, the central and western segments have been identified to have relatively little or sparse lineament structures (Ebong *et al.* 2021a).

Generally, T and k are related linearly which implies that an increase in k can result in a corresponding increase in the value of T. The northeastern portion and locations around major fault zones show relatively high values (i.e., $T > 40\ m^2$/day) and decreased to $>10\ m^2$/day toward the south (Figure 6(d)). Additionally, the migmatite and gneisses within the northeastern part have been intensely fractured resulting in relatively thick and partially saturated formations that can increase T values. Also, the relatively high transmissivity observed can be traced to the presence of localized productive fractures/faults that are connected to some nearby surface water and/or rivers that constantly recharge the semi-confined aquifers. Conversely, locations, where charnockitic rocks abound, show low k and T values, due to its resistance to weathering and fracturing. Furthermore, the transmissivity values derived from the hydro-geoelectrical measurements were correlated with TR (Figure 5(d)) and an empirical model with a correlation coefficient ($R^2 = 0.76$) was obtained.

$$\mathrm{TR} = 38,458(T)^{-1.03} \tag{14}$$

This R^2 value implies that the estimated relationship between these two parameters is good. However, the TR values tend to considerably decrease as T increases because the magnitude of resistance offered by the crystalline basement rock is high, except in VES-21 where the layer electrical resistivities were relatively low and correspond to the thick regolith layer. Hence, the relatively low transmissivity observed within the area under investigation (Figure 6(d)).

5.2. Aquifer potential delineation

The resistivity of the fractured-aquifer formation and the estimated transmissivity were used to delineate aquifer potential zones. Locations with ρ range of 100–214 Ωm, $T > 40$ m^2/day and h of the range of 26–50 m were categorized as having good aquifer potential (Table 4). The locations include VES-1, 2, 6, 7, 8, and 19. Moderate potential aquifer zones were observed within VES-3, 4, 5, 9, 10, 11, 12, 13, 16, 18, 20, and 21 with ρ that range between <143 and 438 Ωm, T that range between <40 and 15 m^2/day and h between 10 and 38 m while poor potential aquifer zones that have ρ that range between 145 and 495 Ωm, $T < 15$ m^2/day and h that range from 8 to 24 m were observed in VES-14, 15, and 17. In general, the groundwater potential classification indicates that a decrease in electrical resistivity values of aquifer formation reflects higher fracture density and water content. Hence, adequate structural elements (i.e., fractures and faults) and thickness of the saturated formation are important factors to also consider in siting productive boreholes within such areas.

6. CONCLUSION

Hydrogeologic and electrical resistivity techniques were used to study the OBC for the purpose of developing empirical models used in predicting aquifer hydraulic parameters and delineating potential aquifer zones. The VES technique applied in this study involved the Schlumberger electrode configuration. This technique provided layer parameters used in computing secondary geoelectrical information (i.e., Dar Zarrouk parameters). The *D-Z* parameters, i.e., longitudinal conductance and TR range between 0.04 and 0.85 Ω^{-1} and between 3,266.64 and 64,338.35 Ωm^2, respectively. These wide variations are due to the intrinsic electrical anisotropic nature of the basement terrain. This variation in electrical anisotropy results from the influence of electrical current flow by some factors like geologic structures (i.e., faults and fractures) and topographic conditions. The combination of these primary and secondary parameters alongside water electrical resistivity measurements, and a few pumping test-derived hydraulic parameters were used to develop empirical models used in evaluating aquifer parameters such as fractional porosity of the fractured-aquifer layer (0.20–0.30), hydraulic conductivity (1.14×10^{-5} to 1.76×10^{-5} m/s), and transmissivity (8.1–91.7 m^2/day). Based on the estimated aquifer parameters, groundwater potential zones were delineated within the study area. The results of this investigation provided good, moderate, and poor groundwater potential zones that were semi-confined (i.e., fractured basement aquifers). Additionally, this approach can be applied in hard rock terrains elsewhere to estimate aquifer parameters and delineate suitable sites for productive boreholes. This study develops empirical models for the estimation of fractured-aquifer hydrogeological, physical, and geohydraulic parameters where pumping test information is limited which enables the delineation of groundwater potential zones required for adequate management of groundwater resources and sustainability.

ACKNOWLEDGEMENT

The first author wishes to thank Prof. I. Othman, General Director of the Syrian Atomic Energy Commission for allowing Prof. J. Asfahani to participate in this research paper.

DATA AVAILABILITY STATEMENT

All relevant data are included in the paper or its Supplementary Information.

CONFLICT OF INTEREST

The authors declare there is no conflict.

REFERENCES

Achtziger-Zupancik, P., Loew, S. & Mariéthoz, G. 2017 A new global database to improve predictions of permeability distribution in crystalline rocks at site scale. *Journal of Geophysical Research: Solid Earth* **122**, 3513–3539. https://doi.org/10.1002/2017JB014106.

Ahmed, T. F., Afzal, M. A., Hashmi, H. N., Yousuf, H. M., Shah, S. U. S. & Khan, M. A. 2022 Electrical resistivity survey by Schlumberger electrode configuration technique for ground water exploration in Pakistan. *Pakistan Journal of Agricultural Research* **35**(3), 558–568.

Akpan, A. E., Ebong, E. D. & Emeka, C. N. 2015 Exploratory assessment of groundwater vulnerability to pollution in Abi, southeastern Nigeria, using geophysical and geologic techniques. *Journal of Environmental Monitoring and Assessment* **187**(4), 4380.

Akpan, A. E., Ekwok, S. E. & Ebong, E. D. 2016 Seasonal reversals in groundwater flow direction and its role in the recurrent Agwagune landslide problem: A geophysical and geological appraisal. *Environmental Earth Sciences* **75**(5), 1–17.

Akpan, A. E., Ekwok, S. E., Ebong, E. D., George, A. M. & Okwueze, E. E. 2018 Coupled geophysical characterization of shallow fluvio-clastic sediments in Agwagune, southeastern Nigeria. *Journal of African Earth Sciences* **143**, 67–78.

Aleke, C. G., Ibuot, J. C. & Obiora, D. N. 2018 Application of electrical resistivity method in estimating geohydraulic properties of a sandy hydrolithofacies: A case study of Ajali Sandstone in Ninth Mile, Enugu State, Nigeria. *Arabian Journal of Geosciences* **11**(12), 322.

Archie, G. E. 1942 The electrical resistivity logs as an aid in determining some reservoir characteristics. *Transactions of the American Institute of Mining and Metallurgical Engineers* **146**, 54–62.

Arétouyap, Z., Bisso, D., Njandjock Nouck, P., Amougou Menkpa, L. E. & Asfahani, J. 2019 Hydrogeophysical characteristics of Pan-African aquifer specified through an alternative approach based on the interpretation of vertical electrical sounding data in the Adamawa Region, Central Africa. *Natural Resources Research* **28**(1), 63–77.

Asfahani, J. & Ahmad, Z. 2020 Estimation of hydraulic parameters by using VES sounding and neural network techniques in the semi-arid Khanasser valley region, Syria. *Contributions to Geophysics and Geodesy* **50**(1), 113–133.

Asfahani, J. & Al-Fares, W. 2021 Alternative vertical electrical sounding technique for hydraulic parameters estimation of the quaternary basaltic aquifer in Deir Al-Adas area, Yarmouk Basin, Southern Syria. *Acta Geophysica* **69**(5), 1901–1918.

Bahammou, Y. A., Benamara, A., Ammar, A., Hrittta, D., Dakir, I. & Bouikbane, H. 2021 Application of vertical electrical sounding resistivity technique to explore groundwater in the Errachidia basin, Morocco. *Groundwater for Sustainable Development* **15**, 100648.

Batte, A. G., Barifaijo, E., Keberu, J. M., Kawule, W., Muwanga, A., Owor, M. & Kisekulo, J. 2010 Correlation of geoelectric data with aquifer parameters to delineate the groundwater potential of hard rock terrain in Central Uganda. *Pure and Applied Geophysics Journal* **167**, 1549–1559.

Bhattacharya, P. K. & Patra, H. P. 1968 *Direct Current Geoelectric Sounding: Principles and Interpretation*. Elsevier Science Publishing Co. Inc., Amsterdam.

Binley, A., 2015 11.08 – tools and techniques: Electrical methods. In: *Treatise on Geophysics* (Schubert, G. ed.). Elsevier, Oxford, pp. 233–259.

Chandra, S., Dewandel, B., Dutta, S. & Ahmed, S. 2010 Geophysical model of geological discontinuities in a granitic aquifer: Analyzing small scale variability of electrical resistivity for groundwater occurrences. *Journal of Applied Geophysics* **71**(4), 137–148.

Chibuike, A., Chukwu, A. C. & Kelechi, O. K. 2023 Efficiency and limitation of vertical electrical sounding in evaluation of groundwater potential in fractured shale terrain: A case study of Abakaliki Area Lower Benue Trough Nigeria. *Environmental Monitoring and Assessment* **195**(1), 158.

Courtois, N., Lachassagne, P., Wyns, R., Blanchin, R., Bougaïré, F. D., Somé, S. & Tapsoba, A. 2010 Large-scale mapping of hard-rock aquifer properties applied to Burkina Faso. *Groundwater* **48**(2), 269–283.

Darko, P. K. & Krásny, J. 2007 Regional Transmissivity Distribution and Groundwater Potential in Hard Rock of Ghana. In Groundwater in Fractured Rocks (pp. 125–136). Boca Raton, FL: CRC Press.

Dewandel, B., Lachassagne, P., Zaidi, F. K. & Chandra, S. 2011 A conceptual hydrodynamic model of a geological discontinuity in hard rock aquifers: Example of a quartz reef in granitic terrain in South India. *Journal of Hydrology* **405**(3–4), 474–487.

Ebong, E. D. 2012 *Electrical Resistivity Investigation of the Spatial Distribution of Soil and Groundwater Salinity in Abi Local Government Area, Cross River State, Nigeria*. *Unpublished* M.Sc Thesis, University of Calabar, Calabar.

Ebong, E. D., Akpan, A. E. & Onwuegbuche, A. A. 2014 Estimation of geohydraulic parameters from fractured shale and sandstone aquifers of Abi (Nigeria) using electrical resistivity and hydrogeologic measurements. *Journal of African Earth Sciences* **96C**, 99–109.

Ebong, E. D., Akpan, A. E., Emeka, C. N. & Urang, J. G. 2017 Groundwater quality assessment using geoelectrical and geochemical approaches: Case study of Abi Area, southeastern Nigeria. *Journal of Applied Water Science* **7**(5), 2463–2478.

Ebong, E. D., Abong, A. A., Ulem, E. B. & Ebong, L. A. 2021a Geoelectrical resistivity and geologic characterization of hydrostructures for groundwater resource appraisal in the Obudu Plateau, southeastern Nigeria. *Journal of Natural Resources Research* **30**(3), 2103–2117.

Ebong, E. D., George, A. M., Ekwok, S. E., Akpan, A. E. & Asfahani, J. 2021b 2D electrical resistivity inversion and ground penetrating radar investigation of near surface cave in New Netim area, southeastern Nigeria. *Acta Geodaetica et Geophysica* **56**(4), 765–780.

Ebong, E. D., Urang, J. G., Melouah, O., Ugi, A. U. & Sule, A. 2023 Near-surface geophysical characterization of gully erosion hazard-prone area in Calabar, southern Nigeria. *Acta Geophysica*. https://doi.org/10.1007/s11600-023-01103-7.

Edem, G. O., Ekwueme, B. N., Ephraim, B. E. & Igonor, E. E. 2016 Preliminary investigation of pegmatites in Obudu Area, southeastern Nigeria, using stream sediments geochemistry. *Global Journal of Pure and Applied Sciences* **22**(2), 167.

Edet, A. E. & Okereke, C. S. 2005 Hydrogeological and hydrochemical character of the regolith aquifer, northern Obudu Plateau, southern Nigeria. *Hydrogeology Journal* **13**(2), 391–415.

Ekwok, S. E., Akpan, A. E., Kudamnya, E. A. & Ebong, E. D. 2020 Assessment of groundwater potential using geophysical data: a case study in parts of Cross River State, south-eastern Nigeria. *Applied Water Science* **10** (6), 1–17.

Ekwueme, B. N. 1990 Rb-Sr age and petrologic features of the Precambrian rocks from Oban massif southeastern Nigeria. *Precambrian Research* **47**, 271–286.

Ekwueme, B. N. 1994 Structural features of southern Obudu Plateau, Bamenda massif, SE Nigeria: Preliminary interpretations. *Journal of Mining Geology* **30**(1), 45–59.

Ekwueme, B. N. 2003 *The Precambrian Geology and Evolution of the Southeastern Nigerian Basement Complex*. University of Calabar Press, Calabar, pp. 1–57.

Etu-Efeotor, J. O. 1997 *Fundamentals of Petroleum Geology*. Paragraphics, Port Harcourt, Nigeria, pp. 51–63.

Freeze, R. A. & Cherry, J. A. 1979 *Groundwater*. Prentice Hall, NJ, USA. (No. 629.1 F7).

George, N. J., Ibuot, J. C., Ekanem, A. M. & George, A. M. 2018 Estimating the indices of inter-transmissibility magnitude of active surficial hydrogeologic units in Itu, Akwa Ibom State, Southern Nigeria. *Arabian Journal of Geosciences* **11**(6), 134.

Gnanachandrasamy, G., Ramkumar, T., Chen, J. Y., Venkatramanan, S., Vasudevan, S. & Selvam, S. 2019 Evaluation of vulnerability zone of a coastal aquifer through GALDIT GIS index techniques. In: Venkatramanan, S., Prasanna, M.V., Chung, S.Y. (Eds.), GIS and Geostatistical Techniques for Groundwater Science. Elsevier, Amsterdam, Netherlands, pp. 209–221.

Gowd, S. S. 2004 Electrical resistivity surveys to delineate groundwater potential aquifers in Peddavanka watershed, Anantapur District, Andhra Pradesh, India. *Journal of Environmental Geology* **46**, 118–131.

Guevara-Mansilla, O., López-Loera, H., Ramos-Leal, J. A., Ventura-Houle, R. & Guevara-Betancourt, R. E. 2020 Characterization of a fractured aquifer through potential geophysics and physicochemical parameters of groundwater samples. *Environmental Earth Sciences* **79**(14), 1–17.

Guevara, H. J. P., Barrientos, J. H., Rodríguez, O. D., Guevara, V. M. P., Cárdenas, O. L. & Torres, M. L. D. G. 2017 Estimation of Hydrological Parameters from Geoelectrical Measurements. In El Shahat, A., Electrical Resistivity and Conductivity. IntechOpen, pp. 83– 95.

Haq, F. U., Naeem, U. A., Ahmad, I., Waseem, M. & Iqbal, M. 2022 Electrical resistivity in the assessment of subsurface lithology and groundwater depth – a case study in Rawalpindi, Pakistan. *Arabian Journal of Geosciences* **15**(18), 1534.

Hassan, W. H., Hussein, H. H. & Nile, B. K. 2022 The effect of climate change on groundwater recharge in unconfined aquifers in the western desert of Iraq. *Groundwater for Sustainable Development* **16**, 100700.

Hussain, Y., Ullah, S. F., Hussain, M. B., Aslam, A. Q., Akhter, G., Martinez-Carvajal, H. & Cárdenas-Soto, M. 2017 Modelling the vulnerability of groundwater to contamination in an unconfined alluvial aquifer in Pakistan. *Environmental Earth Sciences* **76**(2), 84.

Ige, O. O., Ameh, H. O. & Olaleye, I. M. 2021 Borehole inventory, groundwater potential and water quality studies in Ayede Ekiti, Southwestern Nigeria. *Discover Water* **1**(1), 1–20.

Inman, J. R. 1975 Resistivity inversion with ridge regression. *Geophysics* **40**, 798–817.

Karthik, B., Sankar, K., Rajasekar, R., Santhi, D. & Suresh, R. 2022 Electrical resistivity data interpretation for groundwater detection in Manimuktha River Basin, Tamil Nadu, India. *International Journal of Research in Engineering, Science and Management* **5**(1), 189–194.

Kelly, W. E. 1977 Geoelectric sounding for estimating aquifer hydraulic conductivity. *Groundwater* **15**(6), pp. 420–425.

Keller, G. V. 1987 Rock and Mineral Properties, Electromagnetic Methods in Applied Geophysics–Theory, vol. 1. Society of Exploration Geophysicists, pp. 13–51.

K'Orowe, M. O., Nyadawa, M. O., Singh, V. S. & Dhakate, R. 2011 Hydrogeophysical parameter estimation for aquifer characterisation in hard rock environments: A case study from Jangaon sub-watershed, India. *Journal of Oceanography and Marine Science* **2**(3), 50–62.

Kruseman, G. P. & de Ridder, N. A. 1990 *Analysis and Evaluation of Pumping Test Data*. ILRI Publication, (47). Wageningen, Netherlands.

LaBrecque, D. J., Miletto, M., Daily, W., Ramirez, A. & Owen, E. 1996 The effects of noise on Occam's inversion of resistivity tomography data. *Geophysics* **61**(2), 538–548.

Lachassagne, P., Dewandel, B. & Wyns, R. 2021 Hydrogeology of weathered crystalline/hard-rock aquifers – guidelines for the operational survey and management of their groundwater resources. *Hydrogeology Journal* **29**(8), 2561–2594.

Limaye, S. D. 2010 Groundwater development and management in the Deccan Traps (basalts) of western India. *Hydrogeology Journal* **18**(3), 543–558.

Lobo-Ferreira, J. P., Chachadi, A. G., Diamantino, C. & Henriques, M. J. 2005 Assessing aquifer vulnerability to seawater intrusion using GALDIT Method. Part 1: Application to the Portuguese aquifer of Monte Gordo.

Lohman, S. W. 1979 *Groundwater Hydraulics*. U.S Geological Survey paper 708. United States Government Printing Office. Washington.

Mahmud, S., Hamza, S., Irfan, M., Huda, S. N. U., Burke, F. & Qadir, A. 2022 Investigation of groundwater resources using electrical resistivity sounding and Dar Zarrouk parameters for Uthal Balochistan, Pakistan. *Groundwater for Sustainable Development* **17**, 100738.

Maillet, R. 1947 The fundamental equations of electrical prospecting. *Geophysics* **12**(4), 529–556.

Maliva, R. & Missimer, T. 2012 Introduction to aquifer hydraulics. In: Allan, R., Förstner, U., Salomons, W. (Eds.) *Arid Lands Water Evaluation and Management*. Springer, Berlin, Heidelberg, pp. 117–148.

Mazáč, O., Kelly, W. E. & Landa, I. 1985 A hydrogeophysical model for relations between electrical and hydraulic properties of aquifers. *Journal of Hydrology* **79**(1–2), 1–19.

Mhamdi, A., Dhahri, F., Gouasmia, M., Moumni, L. & Mohamed, S. 2015 Groundwater salinization survey of the Upper Cretaceous-Miocene Complexe terminal aquifer in the Sabaa Biar area of southwestern Tunisia. *Journal of African Earth Sciences* **112**, 83–92.

Mondal, N. C. 2021 Geoelectrical signatures for detecting water-bearing zones in a micro-watershed of granitic terrain from Southern India. *Journal of Applied Geophysics* **191**, 104361.
Mondal, N. C., Das, S. N. & Singh, V. S. 2008 Integrated approach for identification of potential groundwater zones in Seethanagaram Mandal of Vizianagaram District, Andhra Pradesh, India. *Journal of Earth System Science* **117**(2), 133–144.
Mondal, N. C., Devi, A. B., Raj, P. A., Ahmed, S. & Jayakumar, K. V. 2016 Estimation of aquifer parameters from surfacial resistivity measurement in a granitic area in Tamil Nadu. *Current Science* **111**(3), 524–534.
Naidu, S., Gupta, G., Shailaja, G. & Tahama, K. 2021 Spatial behavior of the Dar-Zarrouk parameters for exploration and differentiation of water bodies aquifers in parts of Konkan coast of Maharashtra, India. *Journal of Coastal Conservation* **25**(1), 1–9.
Ndubueze, D. N., Igboekwe, M. U. & Ebong, E. D. 2019 Assessment of groundwater potential in Ehime Mbano, southeastern Nigeria. *Journal of Geosciences* **7**(3), 134–144.
Niwas, S. & Singhal, D. C. 1981 Estimation of aquifer transmissivity from Dar-Zarrouk parameters in porous media. *Journal of Hydrology* **50**, 393–399.
Obianwu, V. I., Egor, A. O., Okiwelu, A. A. & Ebong, E. D. 2015 Integrated geophysical studies over parts of Central Cross River State for the determination of groundwater potential and foundation properties of rocks. *Journal of Applied Geology and Geophysics* **3**, 49–64.
Oden, M. I., Okpamu, T. A. & Amah, E. A. 2012 Comparative analysis of fracture lineaments in Oban and Obudu areas, southeastern Nigeria. *Journal of Geography and Geology* **4**(2), 36–47.
Okereke, C. S., Esu, E. O. & Edet, A. E. 1995 Some hydrogeological properties of crystalline basement in the Oban-Obudu highland region southeastern Nigeria. *Bulletin of Engineering Geology and the Environment* **52**, 91–99.
Okonkwo, A. C. & Ugwu, G. Z. 2015 Determination of Dar-Zarrouk parameters for prediction of aquifer protective capacity: A case of Agbani Sandstone Aquifer, Enugu State, Southeastern Nigeria. *International Research Journal of Geology and Mining* **5**(2), 12–19.
Puranik, S. C. 2009 Occurrence and quality characterisation of groundwater in hard rock terrains of Karnataka. *Journal of Geology and Mining Research* **1**(10), 208–213.
Reynolds, J. M. 2011 *An Introduction to Applied and Environmental Geophysics*. John Wiley & Sons, Oxford, pp. 712.
Sanderson, D. J. & Zhang, X. 1999 Critical stress localization of flow associated with deformation of well-fractured rock masses, with implications for mineral deposits. *Geological Society, London, Special Publications* **155**(1), 69–81.
Saravanan, S., Parthasarathy, K. S. S. & Sivaranjani, S. 2019 Assessing coastal aquifer to seawater intrusion: Application of the GALDIT method to the Cuddalore Aquifer, India. In: Ramkumar, M., James R. A., Menier, D., Kumaraswamy K. (Eds.), Coastal Zone Management. Elsevier, Amsterdam, Netherlands, pp. 233–250.
Sarwade, D. V., Singh, V. S., Puranik, S. C. & Mondal, N. C. 2007 Comparative study of analytical and numerical methods for estimation of aquifer parameters: A case study in basaltic terrain. *Journal of Geological Society of India* **70**(6), 1039–1046.
Shapiro, A. M., Ladderud, J. A. & Yager, R. M. 2015 Interpretation of hydraulic conductivity in a fractured-rock aquifer over increasingly larger length dimensions. *Hydrogeology Journal* **23**(7), 1319–1339.
Telford, W. M., Geldart, L. P. & Sheriff, R. E. 1990 *Applied Geophysics*. Cambridge University Press, Cambridge, United Kingdom.
Uhlemann, S., Chambers, J., Falck, W. E., Tirado Alonso, A., Fernández González, J. L. & Espín de Gea, A. 2018 Applying electrical resistivity tomography in ornamental stone mining: Challenges and solutions. *Minerals* **8**(11), 4.
Ukwang, E. E., Ekwueme, B. N. & Horsley, R. J. 2003 Petrology of granulite facies rock in Ukwortung area of Obudu Plateau, southeastern Nigeria. *Global Journal of Geological Sciences* **1**(2), 159–168.
Vander Velpen, B. P. A. 1988 *Resist Version 1.0*. M. Sc Research Project, ITC, Deft, Netherlands.
Vander Velpen, B. P. A. & Sporry, R. J. 1993 RESIST- a computer program to process resistivity sounding data on PC compatibles. *Computers and Geosciences* **19**(5), 691–703.
Vogelgesang, J. A., Holt, N., Schilling, K. E., Gannon, M. & Tassier-Surine, S. 2020 Using high-resolution electrical resistivity to estimate hydraulic conductivity and improve characterization of alluvial aquifers. *Journal of Hydrology* **580**, 123992.
Vukovic, M. & Soro, A. 1992 *Determination of Hydraulic Conductivity of Porous Media From Grain-Size Composition*. Water Resources Publications, Littleton, CO.
Yeboah-Forson, A. & Whitman, D. 2014 Electrical resistivity characterization of anisotropy in the Biscayne Aquifer. *Groundwater* **52**(5), 728–736.
Younger, P. L. 2007 *Groundwater in the Environment: An Introduction*. Blackwell Publishing, MA, London, p. 318.
Youssef, M. A. S. 2020 Geoelectrical analysis for evaluating the aquifer hydraulic characteristics in Ain El-Soukhna area, West Gulf of Suez, Egypt. *NRIAG Journal of Astronomy and Geophysics* **9**(1), 85–98.
Zhu, L., Gong, H., Chen, Y., Li, X., Chang, X. & Cui, Y. 2016 Improved estimation of hydraulic conductivity by combining stochastically simulated hydrofacies with geophysical data. *Scientific Reports* **6**, 22224.
Ziarani, A. S. & Aguilera, R. 2012 Pore-throat radius and tortuosity estimation from formation resistivity data for tight-gas sandstone reservoirs. *Journal of Applied Geophysics* **83**, 65–73.

First received 16 August 2023; accepted in revised form 13 October 2023. Available online 25 October 2023